Additive-controlled Regio-switching in Ni-catalyzed Enantioselective Hydrophosphination of Unactivated Alkenes

Jian Zhou[1], Sichen Tao[1], Xinglong Zhang[2]*, Jun (Joelle) Wang[1]*

[1]Department of Chemistry, Hong Kong Baptist University, Kowloon, Hong Kong, China

[2]Department of Chemistry, The Chinese University of Hong Kong, Shatin, New Territories, Hong Kong, China

Corresponding author. Email: xinglong.zhang@cuhk.edu.hk; junwang@hkbu.edu.hk

Content

8. Computational Studies

8.1 Computational Methods

8.1.1 Conformational sampling

Conformational sampling was performed using Grimme's *CREST* program[11,12], which used metadynamics (MTD) with genetic z-matrix crossing (GC) performed at theGFN2-xTB[13-15] extended semiempirical tight-binding level of theory with *opt=vtight* option. The isolated conformers were used for further density functional theory (DFT) calculations.

8.1.2 Density functional theory (DFT) calculations

Geometry optimizations were carried out using *Gaussian 16* rev. B.01 software[16] in the gas phase using the global-hybrid meta-NGA (nonseparable gradient approximation) MN15 functional[17] and the def2-SVP[18,19] basis set for all atoms. Truhlar's MN15 functional was chosen to study the present system, as this functional has been employed in the studies of a range of organometallic systems with good accuracy[20-27] Minima and transition structures on the potential energy surface (PES) were confirmed as such by harmonic frequency analysis, showing respectively zero and one imaginary frequency. To improve on the accuracy of the corrected Gibbs energy profile, single point (SP) calculations on the gas phase optimized geometries were performed at MN15 with def2-TZVP[18,19] basis set for all atoms in the implicit C-PCM continuum solvation model[28,29] to model the effect of toluene : DMF (0.48 : 0.02) mixed solvent that was used experimentally, on the potential energy surface. Following our previous work[30], a linearly interpolated dielectric constant (ε) value of 1.8764 for the solvent mixture, toluene : DMF = 0.48 : 0.02, was used (2.38 × 0.48 + 36.7 × 0.02). We use simple linear interpolation for generality to other solvent mixtures for future work. To verify the results, and since pure toluene solvent can be used to achieve the same transformation (albeit with reduced yield and selectivity (Table S7), we separately run single point (SP) calculations on the gas phase optimized geometries at MN15/def2-TZVP[8,9] in the implicit SMD solvation model for toluene. We note that the values produced from both levels of theory are consistent with each other and give the same conclusion.

Gibbs energies were evaluated at the reaction temperature of 80 ºC, using Grimme's scheme of quasi-RRHO treatment of vibrational entropies[31], using the GoodVibes code[32]. Vibrational entropies of frequencies below 100 cm^{-1} were obtained according to a free rotor description, using a smooth damping function to interpolate between the two limiting descriptions[31]. The free energies reported in *Gaussian* from gas-phase optimization were further corrected using standard concentration of 1 mol/L[33], which were used in solvation calculations, instead of the gas-phase 1atm used by default in the *Gaussian* program.

Unless otherwise stated, the final corrected Gibbs energy C-PCM(toluene-DMF)-MN15/def2-TZVP//MN15/def2-SVP is used for discussion. The Gibbs energies in SMD(toluene)-MN15/def2-TZVP//MN15/def2-SVP are included in square brackets. All Gibbs energy values in the text and figures are quoted in kcal mol^{-1}.

Optimized structures and molecular orbitals are visualized using *PyMOL* software[34].

8.2 Model reactions

Scheme S1 shows the model reaction that we used for computational studies of the reaction mechanism for the present reaction. Using pyridine-3-sulfonic acid (reaction on the left), no anti-Markovnikov product was observed and the Markovnikov product was formed in 73% yield with 99% ee. On the other hand, using 3,5-difluorophenol (reaction on the right), only anti-Markovnikov product was formed and no Markovnikov product was observed.

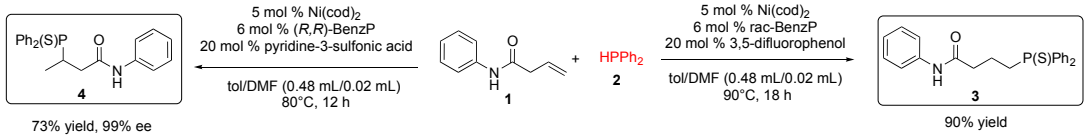

Scheme S1. Model reaction used in computational modelling.

8.3 Conformational Considerations

The bisphosphine ligated Ni-complex where the olefin coordinates via C=C double bond was conformationally sampled to locate the most stable species. We note that, due to the chiral nature of the bisphosphine ligand, the C=C bond can coordinate in two different orientations. The DFT optimized structures of these two coordination modes

are shown in Figure S1. Using each of these structures (**INT1** and **INT1'**) as an initial guess and running the CREST conformational sampling, the results both converge to the same most stable structure, **INT1** after DFT optimization; in other words, CREST only locates one form of the conformer as the most stable structure on the GFN2-xTB potential energy surface, despite having two different initial guess structures. We note that in an initial guess structure where the O atom of the substrate is coordinated to Ni center in **INT1**, the optimized structure has O that is uncoordinated (Figure S1). The amide O atom in **INT1** has a non-covalent interaction with the C–H bond of the *tert*-butyl group on the ligand. On the other hand, in **INT1'**, the amide O atom interacts with Ni center to form an elongated Ni–O bond of 2.44 Å. Interestingly, despite this, **INT1'** is higher in Gibbs energy than **INT1** by 4.5 [4.0] kcal/mol.

INT1	**INT1'**
ΔG = 0.0 [0.0]	ΔG = 4.5 [4.0]
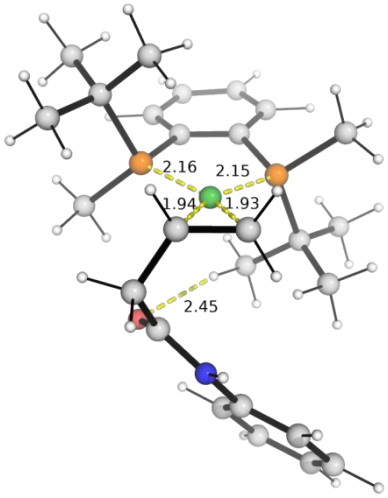	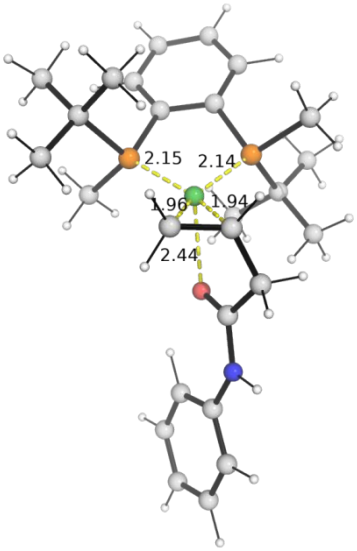
INT1o	
ΔG = 26.7 [26.4]	

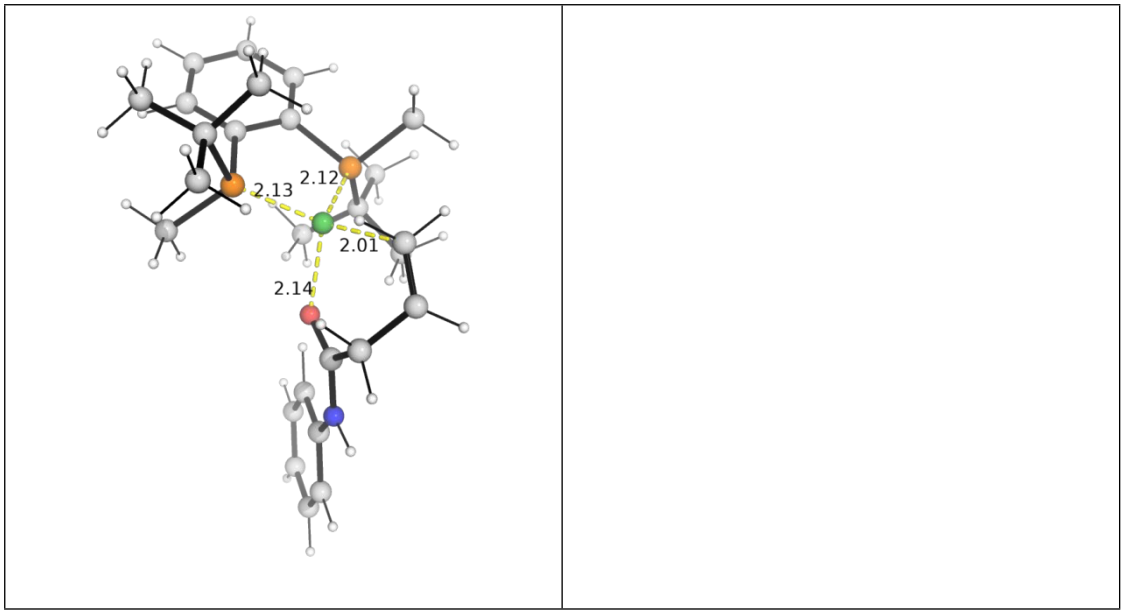

Figure S1. DFT-optimized structures of different conformers of substrate bound to the Ni catalyst. Gibbs energies are given in C-PCM(toluene-DMF)[SMD(toluene)]-MN15/def2-TZVP//MN15/def2-SVP level of theories.

We also try to start from a square planar guess structure where the amide O atom coordinates to the Ni center directly. The optimized structure, **IN1o**, is much higher in energy, by 26.7 [26.4] kcal/mol, than **INT1**, thus, it is thermodynamically less favorable to form O-coordinated **INT1o**.

8.4 Reactivity with pyridine-3-sulfonic acid

As a note, for structures involved in the reaction with pyridine-3-sulfonic acid, the suffix "A" is added after the number. For example, **TS1** leading from **INT1** in this reaction will be denoted **TS1A** and **TS1'** leading from **INT1'** will be denoted as **TS1A'**.

8.4.1 Protonation step

After conformational sampling, we see that for substrate **INT1**, pyridine-3-sulfonic acid can protonate either the terminal carbon of the olefin, via **TS1A_Cterm**, or the internal carbon of the olefin, via **TS1A_Cin** (Figure S3). Alternatively, it can also protonate either carbon of the olefin coordinated in **INT1'**, via **TS1A'_Cterm** or **TS1A'_Cterm**. We located all these TSs and found that protonation of the terminal carbon via **TS1A_Cterm** has the lowest barrier, at 9.5 [11.0] kcal/mol, whereas the protonation of internal carbon via **TS1A'_Cin** has a higher barrier, at 11.6 [13.0] kcal/mol (Figure

S4). This barrier difference of 2.1 [2.0] kcal/mol ($\Delta\Delta G^{\ddagger}$) translates to a d.r. of about 20 : 1 at the reaction temperature of 80ºC, using simple transition state theory.

It is worth noting that the protonation from the approach direction of least steric hinderance (methyl group instead of tert-butyl group) is more favourable than from the other direction (tert-butyl group instead of methyl group). For example, comparing **TS1A_Cterm** and **TS1A_Cin**, the former has a lower barrier than the latter; similarly, comparing **TS1A'_Cin** and **TS1A'_Cterm**, the former has a lower barrier than the latter. In both **TS1A_Cterm** and **TS1A'_Cin**, protonation occurs from the right hand side, whereas in **TS1A_Cin** and **TS1A'_Cterm**, protonation occurs from the left hand side. Structurally, protonation from the right hand side (**TS1A_Cterm** and **TS1A'_Cin**) preserves the planar structure of Ni coordination whereas protonation from the left hand side (**TS1A_Cin** and **TS1A'_Cterm**) distorts the square planar geometry, thus introducing more strains, resulting in elevated activation barriers.

Looking at the conformers of the transition states, we observe favorable interaction between C–H bond of on the *tert*-butyl group and the amide oxygen atom in many TS structures. It is also possible that the amide N–H bond coordinates to Ni-center to stabilize the transition state. The lowest energy TS, **TS1A_Cterm**, may undergo an inner-sphere protonation where an oxygen atom on the sulfone group coordinates to Ni-center at a distance of 2.92Å, while another oxygen atom carries out deprotonation.

TS1A_Cterm	**TS1A_Cterm_c2**
$\Delta G^{\ddagger}$ = 9.5 [11.0]	$\Delta G^{\ddagger}$ = 9.8 [11.3]

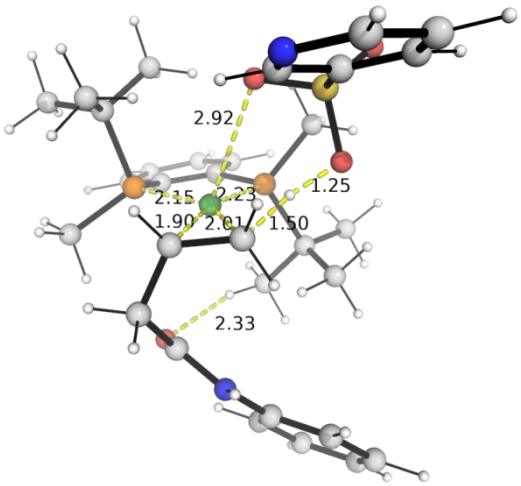	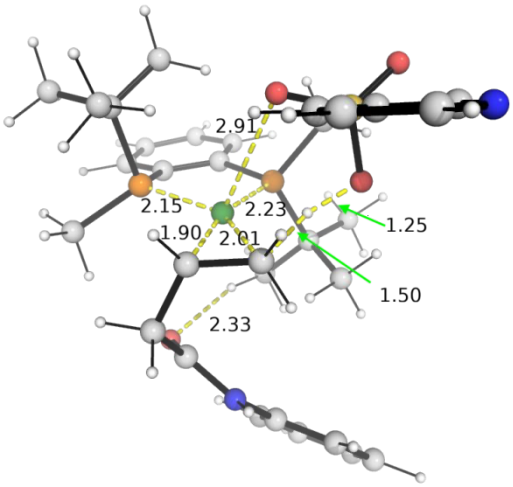
TS1A_Cterm_c3	**TS1A_Cterm_c4**
$\Delta G^{\ddagger}$ = 10.1 [11.0]	$\Delta G^{\ddagger}$ = 12.5 [13.1]
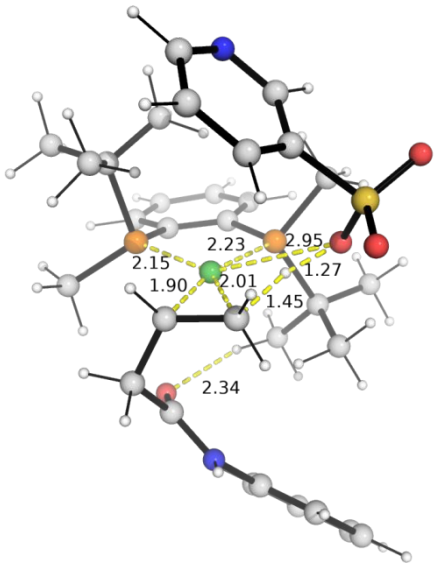	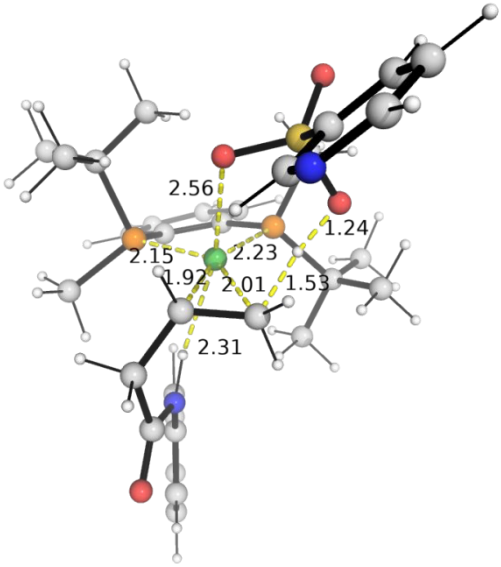
TS1A_Cin	**TS1A'_Cterm**
$\Delta G^{\ddagger}$ = 16.9 [18.0]	$\Delta G^{\ddagger}$ = 19.2 [20.1]

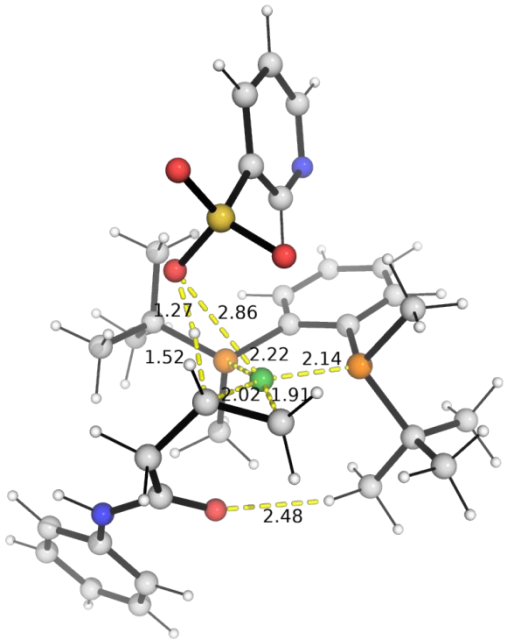	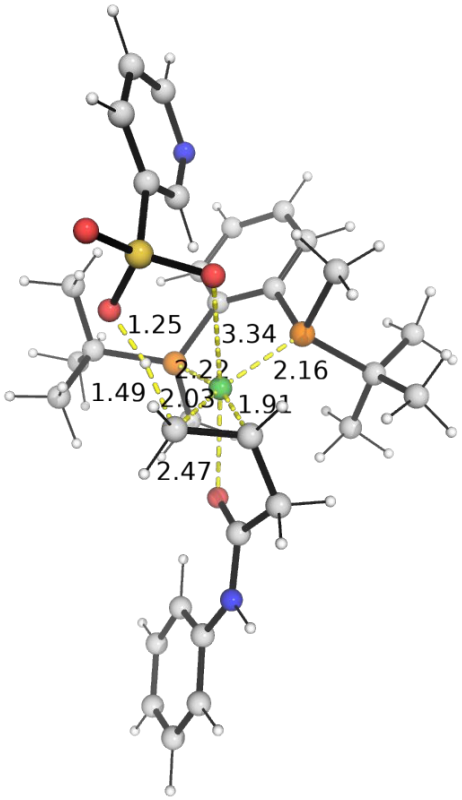
TS1A'_Cin	**TS1A'_Cin_c2**
$\Delta G^{\ddagger}$ = 11.6 [13.0]	$\Delta G^{\ddagger}$ = 13.0 [13.7]
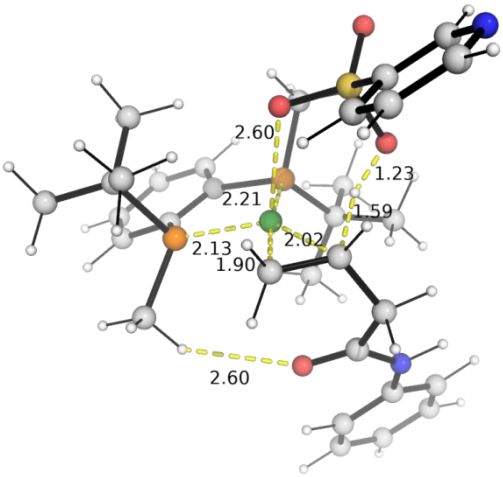	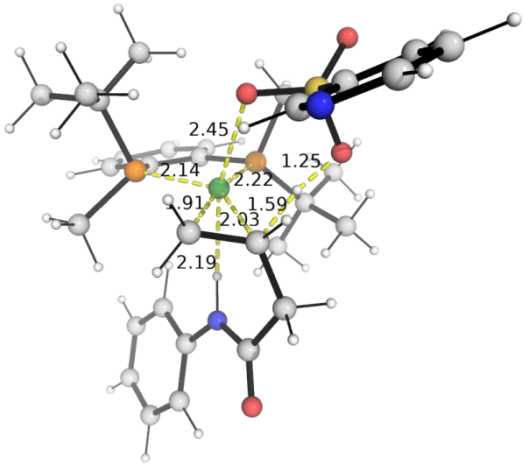
TS1A'_Cin_c3	
$\Delta G^{\ddagger}$ = 14.0 [15.4]	

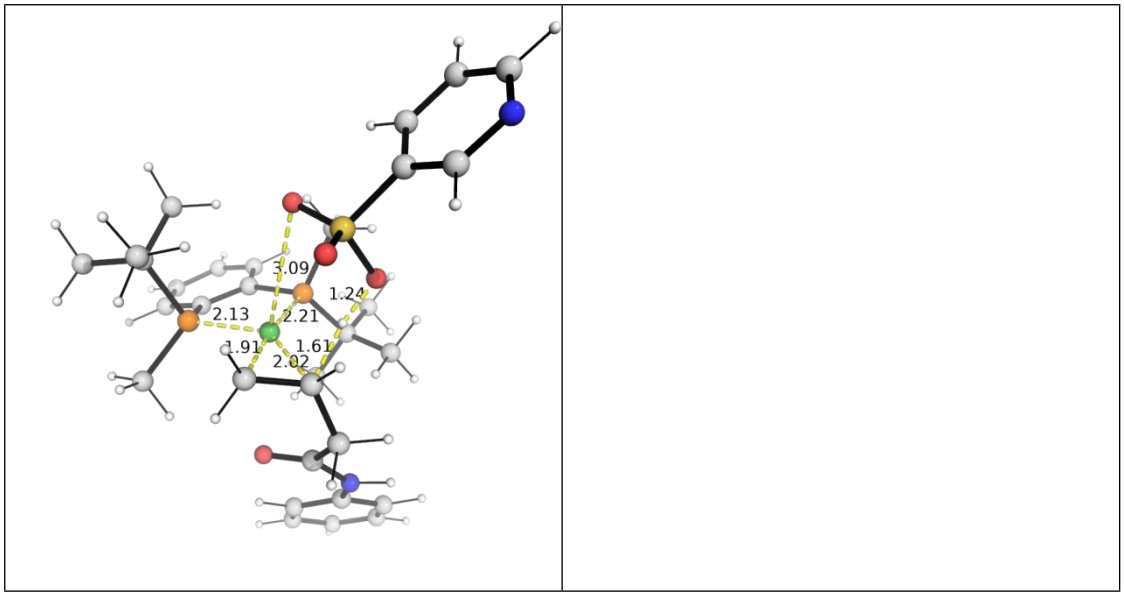

Figure S2. DFT-optimized structures of different conformers of first C–C bond formation transition states (TSs) using pyridine-3-sulfonic acid as the proton source. Gibbs energies relative are given relative to the ground state of **INT1**. Gibbs energies are given in C-PCM(toluene-DMF)[SMD(toluene)]-MN15/def2-TZVP//MN15/def2-SVP level of theories.

8.4.2 Competing transition states

We further analyze the factors influencing the selectivities by comparing the frontier molecular orbitals (FMOs), non-covalent interactions and distortion-interaction analysis in the lowest energy competing TSs, **TS1A_Cterm**, **TS1A_Cin**, **TS1A'_Cterm** and **TS1A'_Cin**. The results are shown in Figure S3 and Table S8.

	TS1A_Cterm	**TS1A_Cin**
barrier	$\Delta G^{\ddagger}$ = 9.5 [11.0]	$\Delta G^{\ddagger}$ = 16.9 [18.0]

DFT Structure	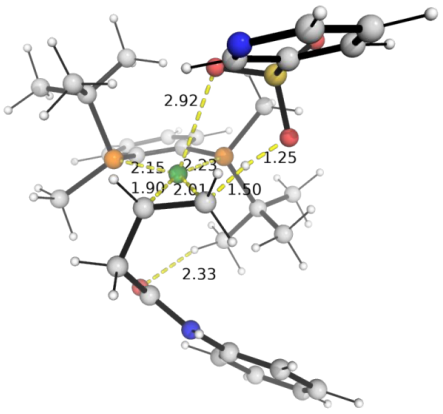	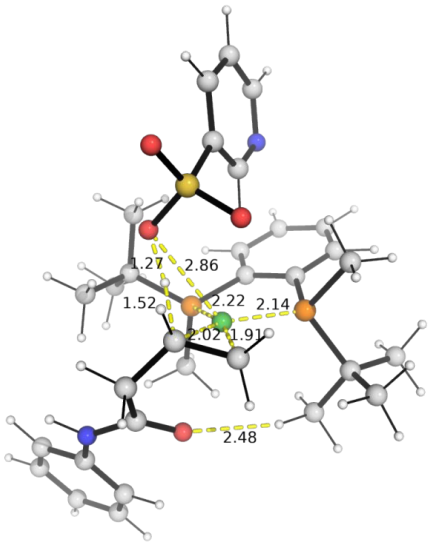
HOMO	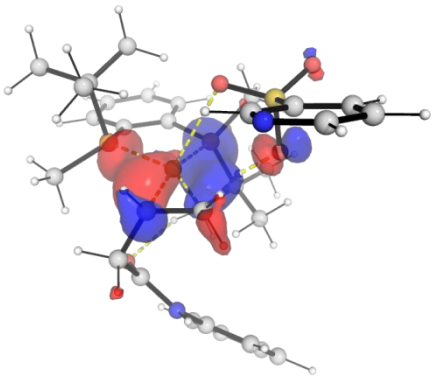	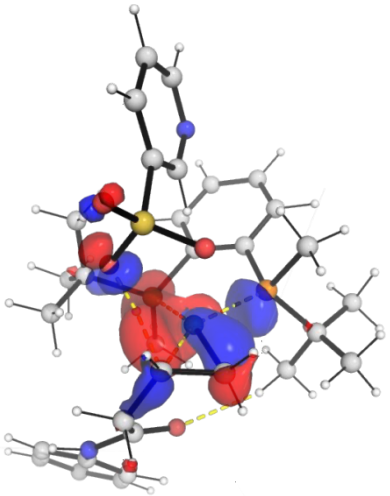
LUMO	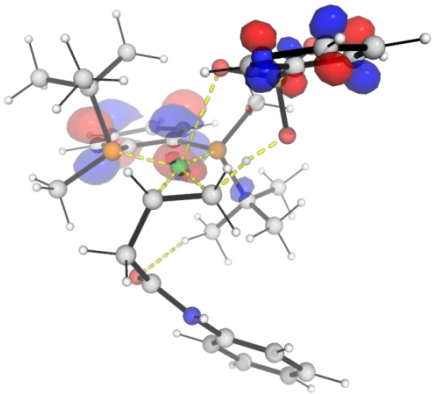	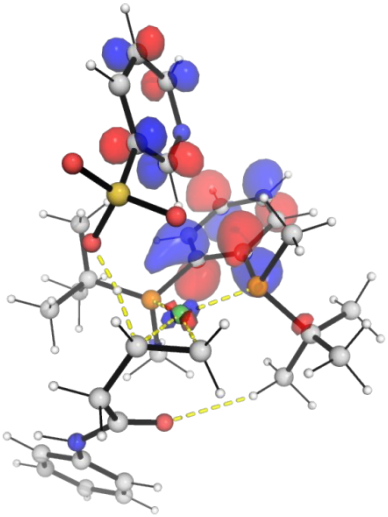

NCI	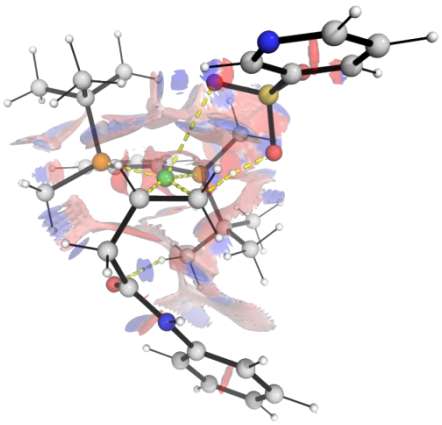	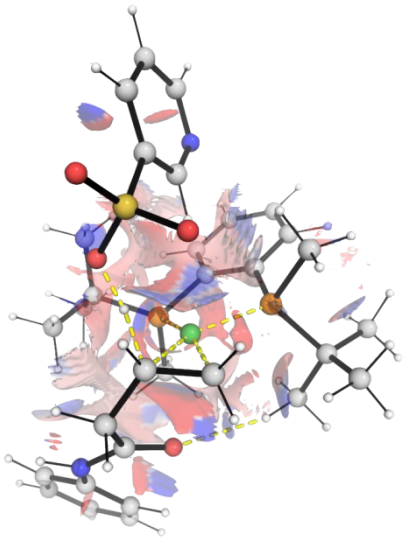
		
	TS1A'_Cterm	**TS1A'_Cin**
barrier	$\Delta G^{\ddagger}$ = 19.2 [20.1]	$\Delta G^{\ddagger}$ = 11.6 [13.0]
DFT Structure	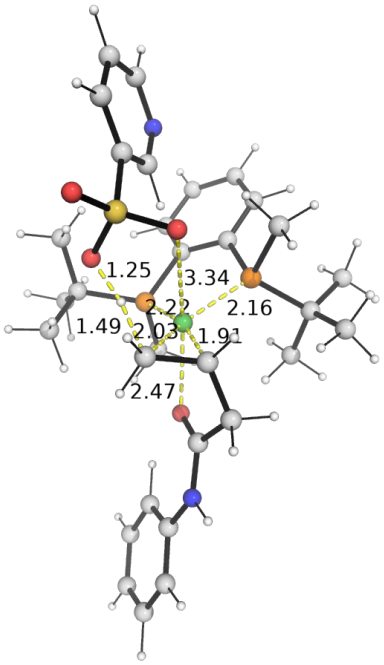	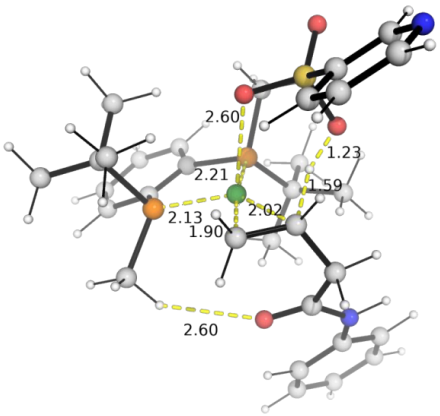

HOMO	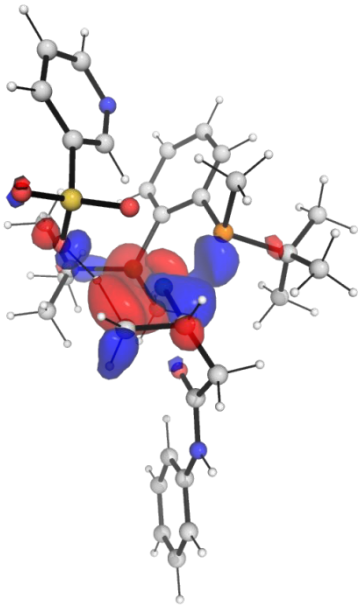	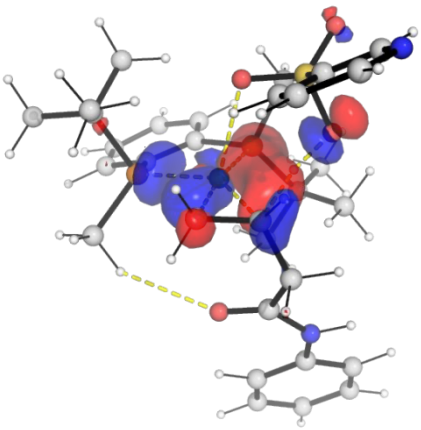
LUMO	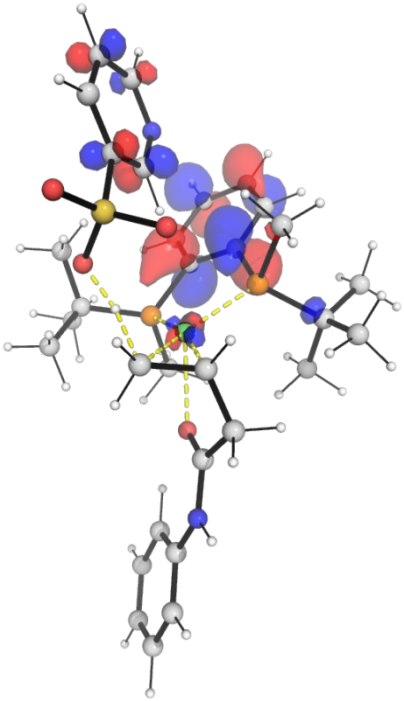	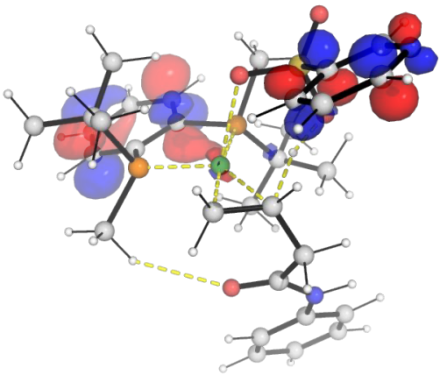

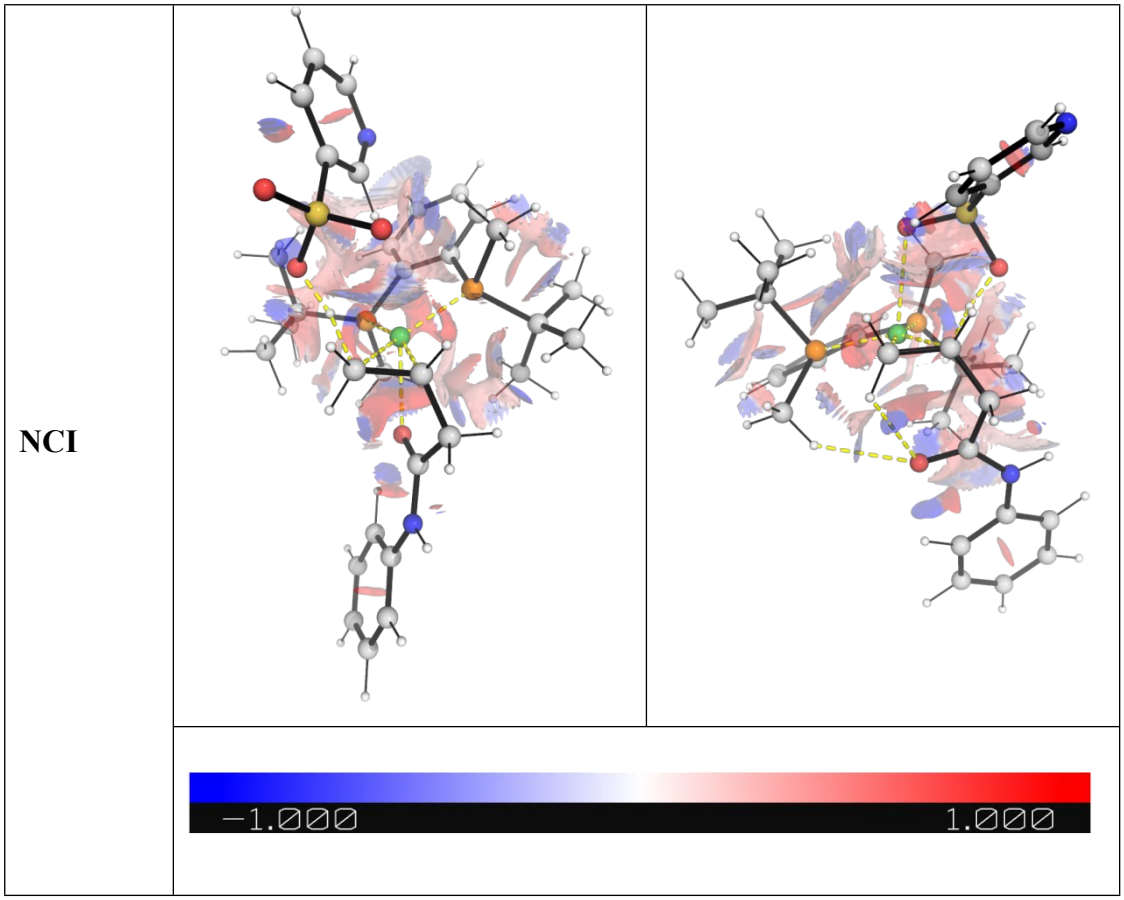

Figure S3. DFT-optimized structures, frontier molecular orbitals (HOMO and LUMO) and non-covalent interaction (NCI) plots for the lowest barrier transition state for the first C–C bond formation transition states (TSs) using pyridine-3-sulfonic acid as the proton source.

Distortion-interaction[35,36], analysis is applied to key TSs to discern the factors affecting regioselectivity. The transition state structures are decomposed by dividing the acid and the olefin-bound Ni-species as components. Single point calculations at C-PCM(toluene-DMF) solvent correction were applied performed at M06-2x/def2-TZVP level of theory to obtain distortion and interaction energies. The distortion energy is given by:

$$E_{dist} = E_{TS,frag1} + E_{TS,frag2} - (E_{eq,frag1} + E_{eq,frag2})$$

where *TS,frag1,2* represent individual fragments in their distorted transition state geometries; and *eq,frag1,2* represent individual fragments in their optimized, equilibrium ground-state geometries; the interaction energy is given by:

$$E_{int} = E_{TS} - (E_{TS,frag1} + E_{TS,frag2})$$

which accounts for the stabilizing interactions (e.g., electrostatic, orbital, dispersion) between the distorted fragments in the TS.

Thus, the total activation energy is given by:

$$\Delta E^{\ddagger} = E_{dist} + E_{int.}$$

Note that this single point activation energy and the activation energy differences $\Delta\Delta E^{\ddagger}$ between the major and minor TSs may be different from the Gibbs energy differences $\Delta\Delta G^{\ddagger}$ that is computed fully (including vibrational frequencies analysis) at C-PCM(toluene-DMF)-MN15/def2-TZVP//MN15/def2-SVP level of theory.

Table S8. Distortion-interaction analysis for the protonation step using pyridine-3-sulfonic acid.

Transition State	$\Delta E^{\ddagger}$	E_{dist}	E_{int}
TS1A_Cterm	-5.4	37.1	-42.5
TS1A_Cin	3.0	48.5	-45.5
TS1A'_Cterm	5.7	49.5	-43.8
TS1A'_Cin	-2.7	39.6	-42.3

This analysis shows that **TS1A_Cterm** has the lowest barrier and is more stable than **TS1A_Cin** by 8.4 kcal/mol, which results from much lower distortion energy, by 11.4 kcal/mol, when the two components approach each other despite the interaction energy that is 3.0 kcal/mol less stabilised. For the protonation of **INT1'**, **TS1A'_Cin** has a lower barrier by 8.4 kcal/mol than **TS1A'_Cterm**, due to the former having much lower distortion energy, by 9.9 kcal/mol, although the interaction energy is slightly less stable, by 1.5 kcal/mol. Thus, the protonation from the approach direction of least steric hinderance (methyl group instead of tert-butyl group) is more favourable (**TS1A_Cterm** and **TS1A'_Cin**) than from the other direction (tert-butyl group instead of methyl group, **TS1A_Cin** and **TS1A'_Cterm**).

In terms of regioselectivity outcome, **TS1A_Cterm** is favoured over **TS1A'_Cin**, by $\Delta\Delta E^{\ddagger} = 2.7$ kcal/mol, primarily due to the smaller distortion in the former than the latter, by 2.5 kcal/mol, whereas the interaction E_{int} is similar in both TSs.

8.4.3 Oxidative addition of O–H of pyridine-3-sulfonic acid to Nickel

The possibility of oxidative addition of O–H of pyridine-3-sulfonic acid to nickel was explored, however, in the process of TS search and the optimization of a potential Ni–H species, it was shown that such Ni–H species could not be formed and that the H atom on Ni-center will add to olefin C=C bond upon geometry optimization, even if we started with a guess Ni–H structure.

8.4.4 Reductive elimination step

TS2A	
$\Delta G^{\ddagger}$ = -13.9 [-11.0]	
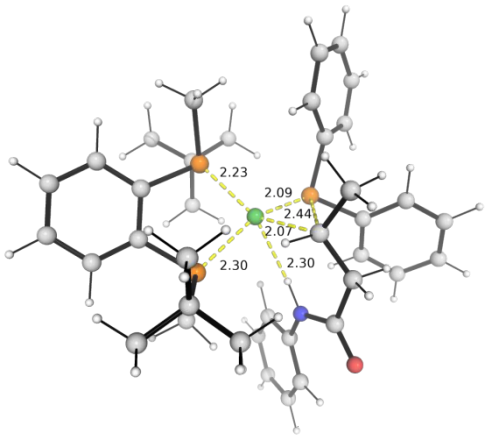	

Figure S4. DFT-optimized structures of the reductive elimination step, **TS2A**.

8.5 Reactivity with 3,5-difluorophenol

For the reaction with 3,5-difluorophenol additive, the suffix "B" is added after the number. For example, **TS1** leading from **INT1** in this reaction will be denoted **TS1B** and **TS1'** leading from **INT1'** will be denoted as **TS1B'**.

8.5.1 Protonation step

Similar to the protonation by pyridine-3-sulfonic acid discussed in the previous section, for **INT1**, the protonation of olefin can occur at either carbon of the C=C bond, via **TS1B_Cterm** and **TS1B_Cin**, Figure S5; for **INT1'**, via **TS1B'_Cterm** and

TS1B'_Cin, Figure S5. As for pyridine-3-sulfonic acid, the protonation from the right hand side has lower barriers than from the left hand side (approach of least steric hinderance). Using 3,5-difluorophenol, the protonation of internal olefin on **INT1'**, via **TS1B'_Cin**, has the lowest barrier, at 24.3 [25.2] kcal/mol. On the other hand, the protonation of terminal olefin has a barrier of 30.1 [30.6] kcal/mol, via **TS1B_Cterm**. This barrier difference of 5.8 [5.4] kcal/mol ($\Delta\Delta G^{\ddagger}$) translates to a d.r. of about 2200–3900 : 1 at the reaction temperature of 80ºC, using simple transition state theory, indicating that protonation by 3,5-difluorophenol predominantly occurs on terminal carbon of the C=C bond of the substrate.

TS1B_Cterm	**TS1B_Cin**
$\Delta G^{\ddagger}$ = 30.1 [30.6]	$\Delta G^{\ddagger}$ = 31.7 [31.1]
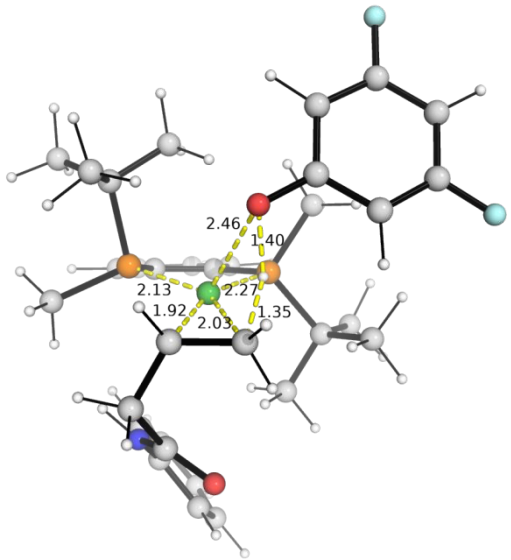	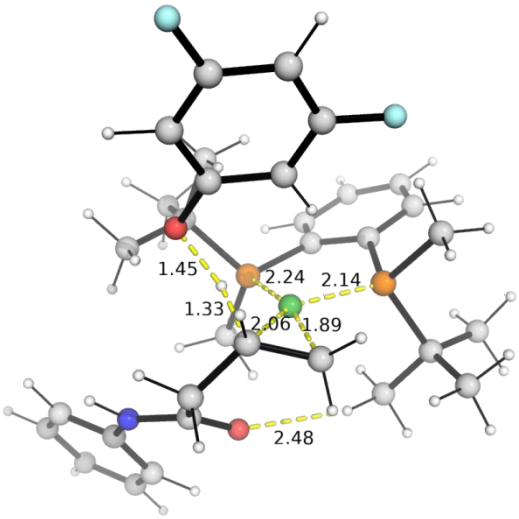
TS1B_Cin_c2	**TS1B_Cin_c3**
$\Delta G^{\ddagger}$ = 31.7 [31.9]	$\Delta G^{\ddagger}$ = 31.7 [33.1]

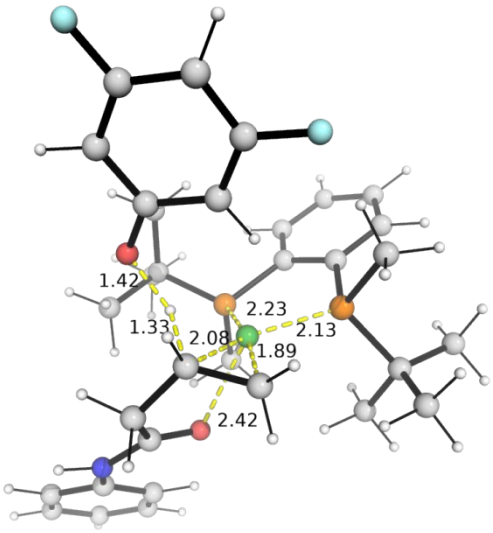	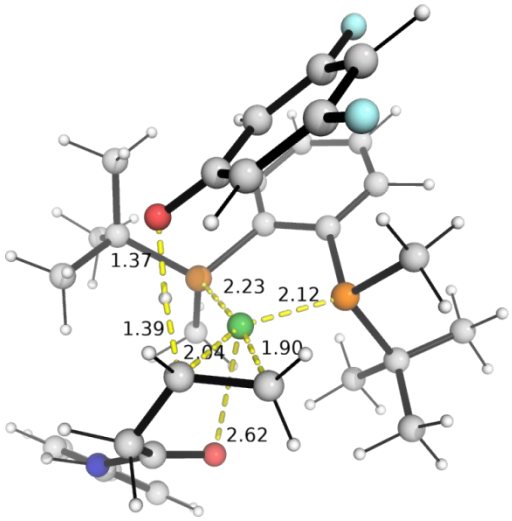
TS1B_Cin_c4	**TS1B'_Cterm**
$\Delta G^{\ddagger}$ = 34.2 [35.6]	$\Delta G^{\ddagger}$ = 32.2 [33.0]
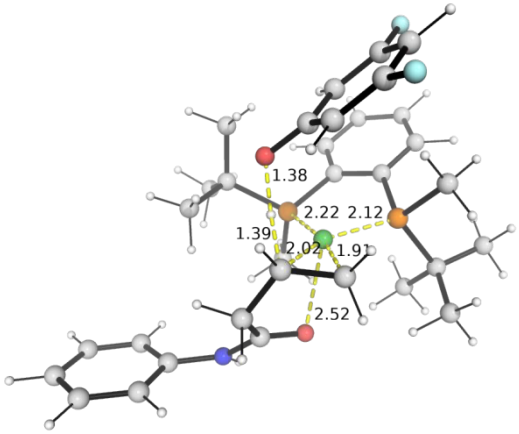	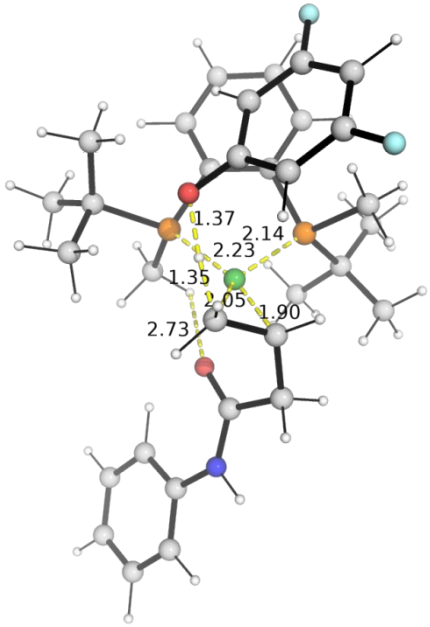
TS1B'_Cterm_c2	**TS1B'_Cterm_c3**
$\Delta G^{\ddagger}$ = 34.0 [35.6]	$\Delta G^{\ddagger}$ = 32.2 [33.0]

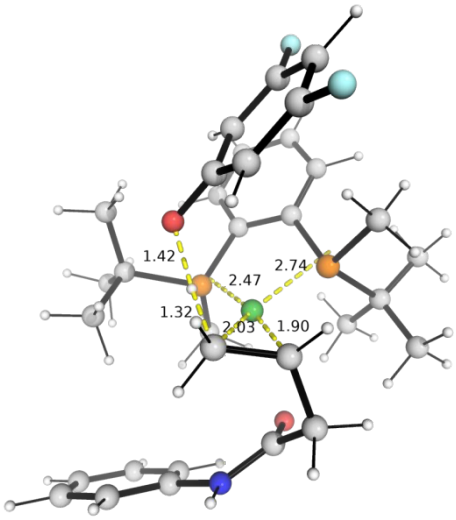	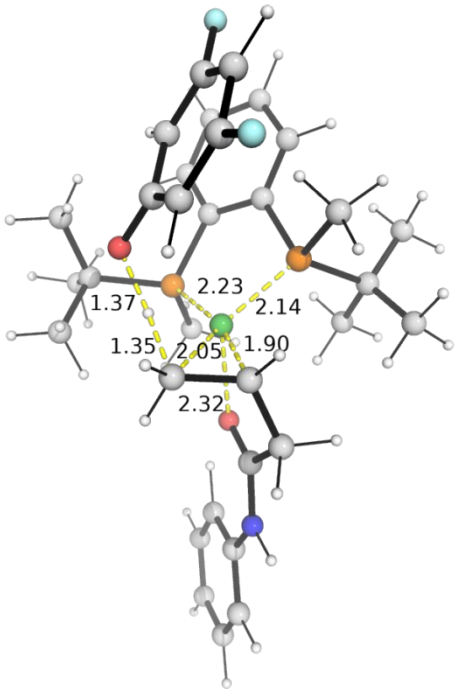
TS1B'_Cin	**TS1B'_Cin_c2**
$\Delta G^{\ddagger}$ = 24.3 [25.2]	$\Delta G^{\ddagger}$ = 26.4 [27.7]
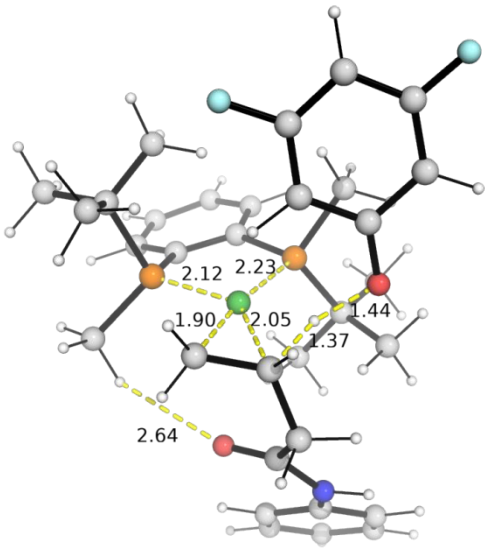	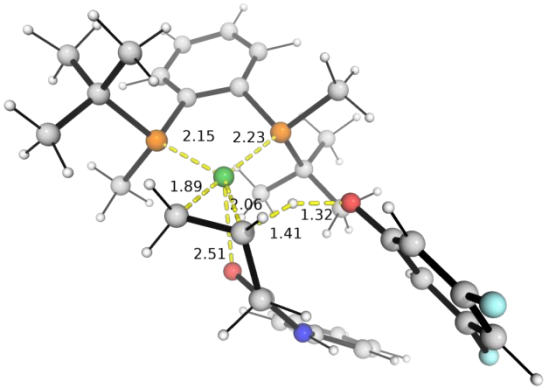
TS1B'_Cin_c3	
$\Delta G^{\ddagger}$ = 31.8 [32.3]	

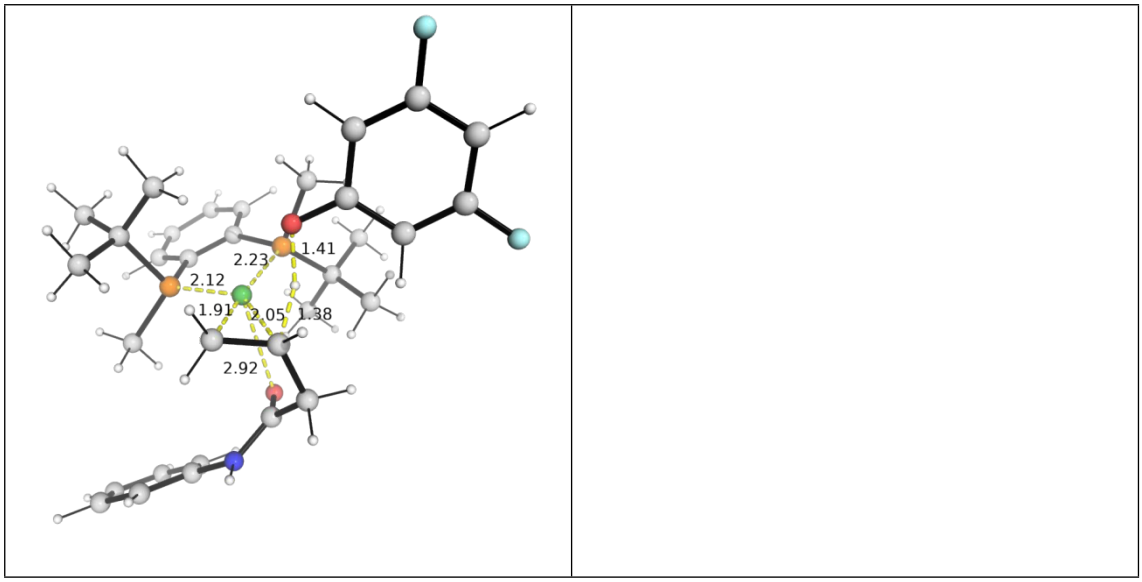

Figure S5. DFT-optimized structures of different conformers of first C–C bond formation transition states (TSs) using 3,5-difluorophenol as the proton source. Gibbs energies relative are given relative to the ground state of **INT1**. Gibbs energies are given in C-PCM(toluene-DMF)[SMD(toluene)]-MN15/def2-TZVP//MN15/def2-SVP level of theories.

8.5.2 Competing transition states

We further analyze the factors influencing the selectivities by comparing the frontier molecular orbitals (FMOs), non-covalent interactions and distortion-interaction analysis in the lowest energy competing TSs, **TS1B_Cterm**, **TS1B_Cin**, **TS1B'_Cterm** and **TS1B'_Cin**. The results are shown in Figure S6 and Table S9.

	TS1B_Cterm	**TS1B_Cin**
barrier	$\Delta G^{\ddagger}$ = 30.1 [30.6]	$\Delta G^{\ddagger}$ = 31.7 [31.1]

DFT Structure	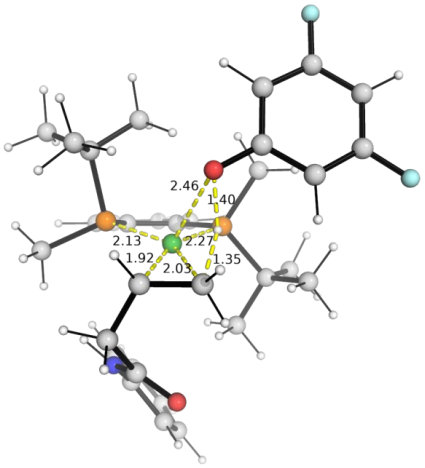	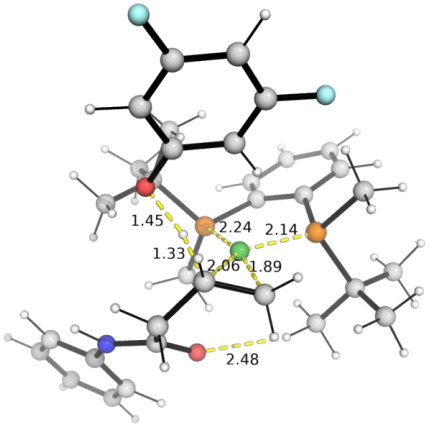
HOMO	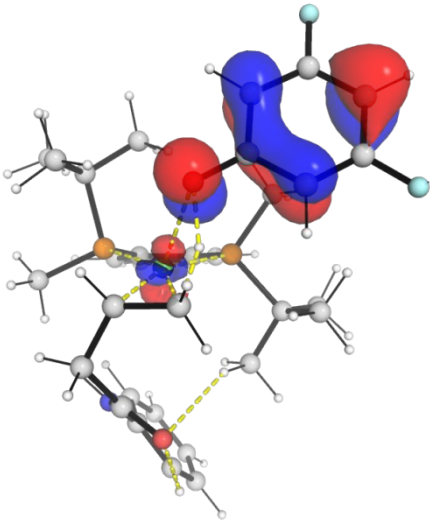	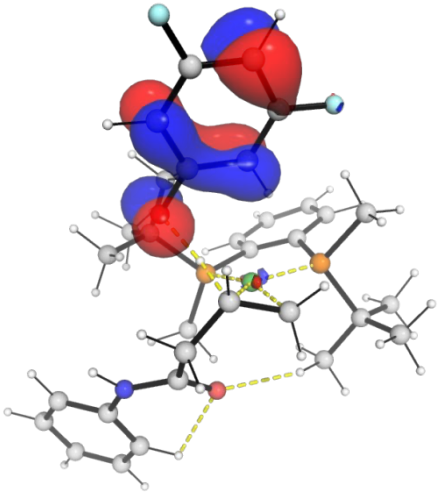
LUMO	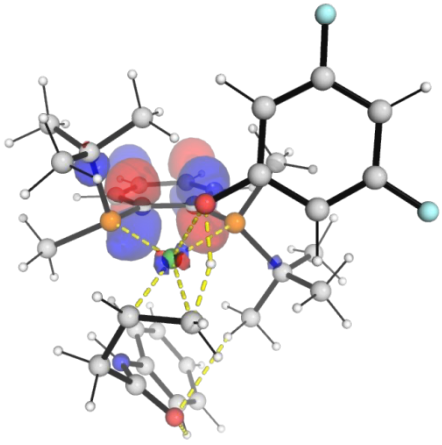	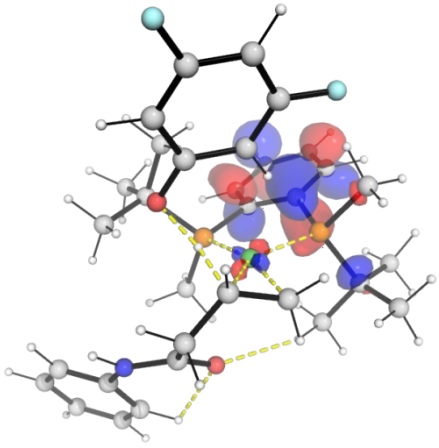

NCI	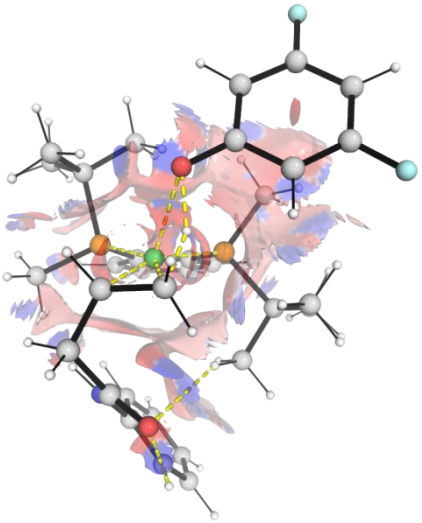	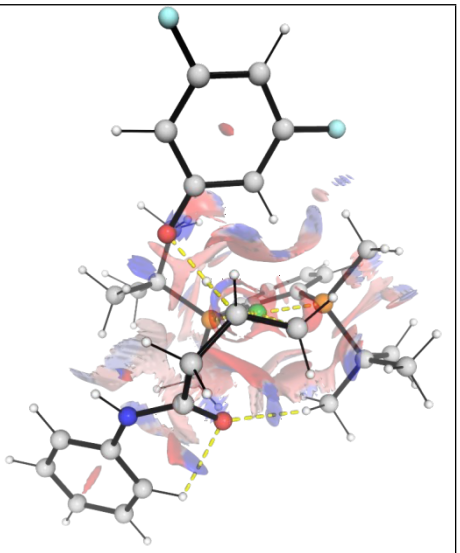
		
	TS1B'_Cterm	**TS1B'_Cin**
barrier	$\Delta G^{\ddagger}$ = 32.2 [33.0]	$\Delta G^{\ddagger}$ = 24.3 [25.2]
DFT Structure	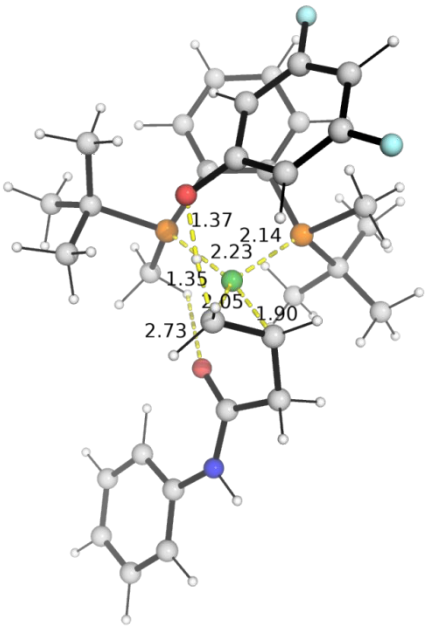	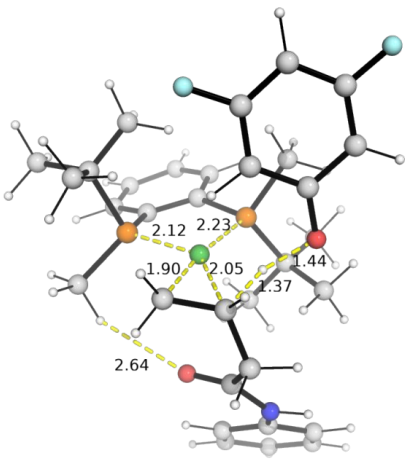

HOMO	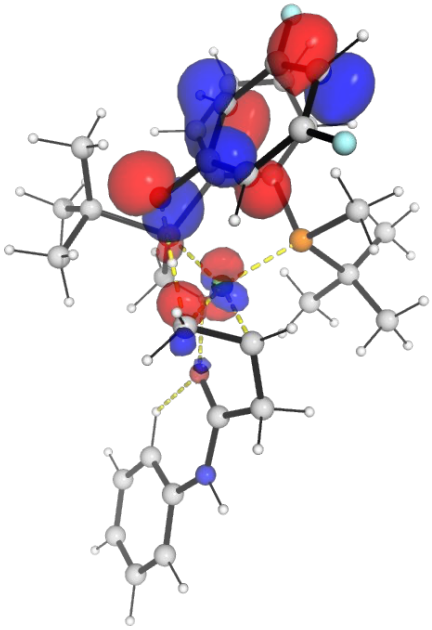	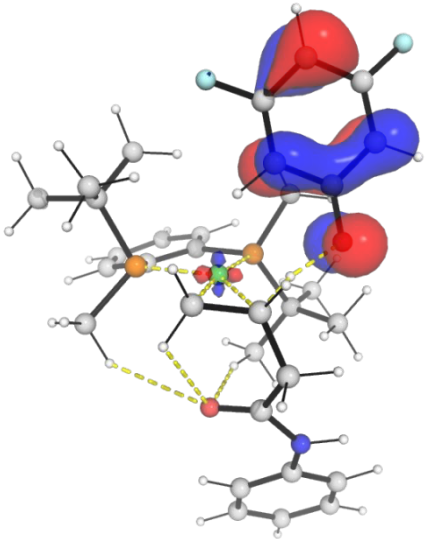
LUMO	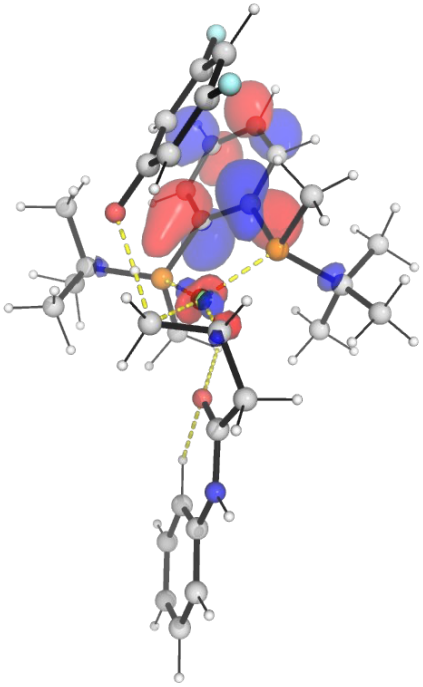	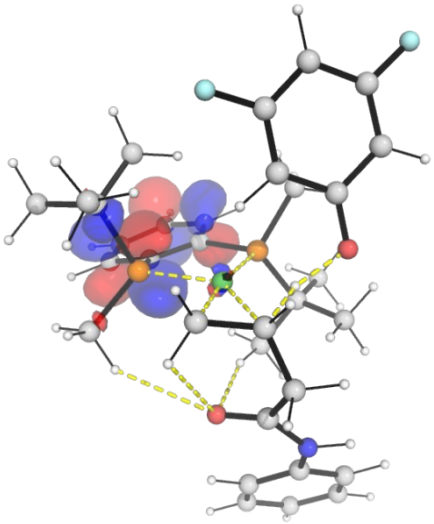

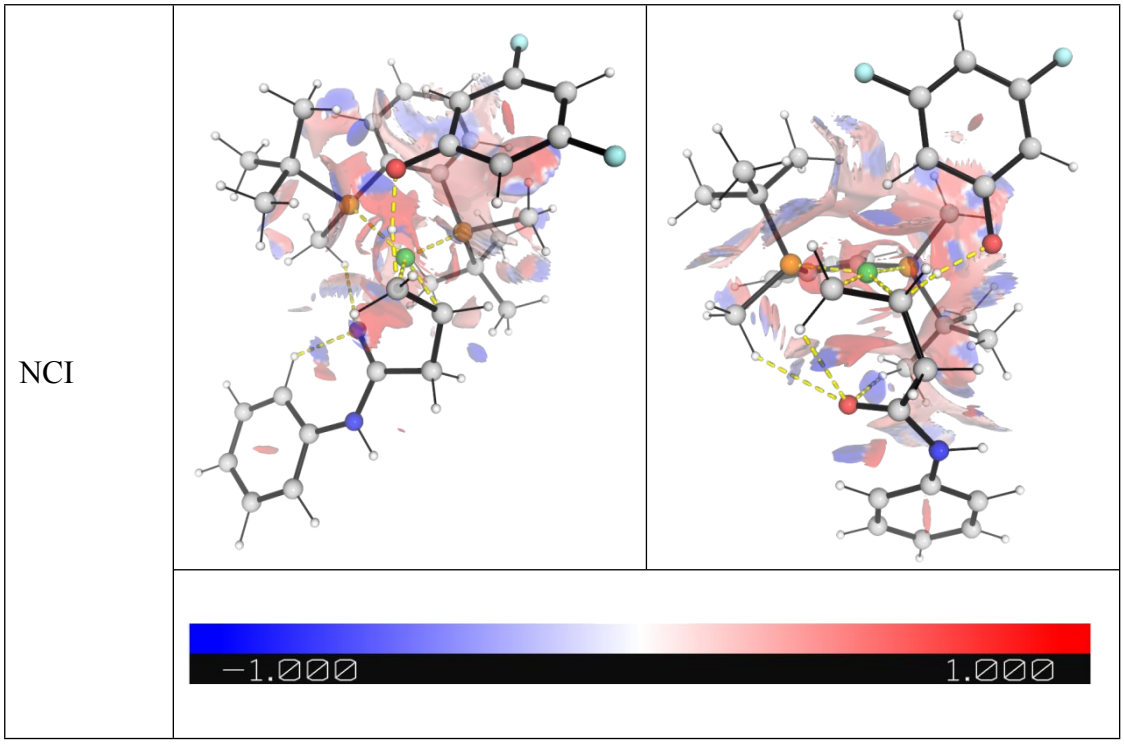

Figure S6. DFT-optimized structures, frontier molecular orbitals (HOMO and LUMO) and non-covalent interaction (NCI) plots for the lowest barrier transition state for the first C–C bond formation transition states (TSs) using 3,5-difluorophenol as the proton source.

As before, distortion-interaction[35,36] analysis is applied to key TSs to discern the factors affecting regioselectivity. The transition state structures are decomposed by dividing 3,5-difluorophenol and the olefin-bound Ni-species as components. Single point calculations at C-PCM(toluene-DMF) solvent correction were applied performed at M06-2x/def2-TZVP level of theory to obtain distortion and interaction energies. The results are given in Table S9.

Table S9. Distortion-interaction analysis for the protonation step using 3,5-difluorophenol.

Transition State	$\Delta E^{\ddagger}$	E_{dist}	E_{int}
TS1B_Cterm	15.2	66.1	-50.9
TS1B_Cin	18.1	75.7	-57.6
TS1B'_Cterm	19.4	72.0	-52.6
TS1B'_Cin	10.0	70.2	-60.2

This analysis shows the protonation of **INT1'** via **TS1B'_Cin** has the lowest barrier, and is more stable than **TS1B'_Cterm** by 9.4 kcal/mol, which results from both lower distortion energy, by 1.8 kcal/mol, and the much more stablized interaction energy, by 7.6 kcal/mol. For the protonation of **INT1**, **TS1B_Cterm** has a lower barrier by 2.9 kcal/mol than **TS1B_Cin**, due to the former having much lower distortion energy, by 9.6 kcal/mol, although the interaction energy is slightly less stable, by 6.7 kcal/mol. As before, the protonation from the approach direction of least steric hinderance (methyl group instead of tert-butyl group) is more favourable (**TS1B_Cterm** and **TS1B'_Cin**) than from the other direction (tert-butyl group instead of methyl group, **TS1B_Cin** and **TS1B'_Cterm**).

In terms of regioselectivity outcome, **TS1B'_Cin** is favoured over **TS1B_Cterm**, by $\Delta\Delta E^{\ddagger}$ = 5.2 kcal/mol, primarily due to the much better stabilization interactions, by 9.3 kcal/mol in **TS1B'_Cin** than in **TS1B_Cterm**, despite the larger distortion in **TS1B'_Cin** than in **TS1B_Cterm**, by 4.1 kcal/mol.

8.5.3 Oxidative addition of O–H of 3,5-difluorophenol to Nickel

Similarly, the possibility of oxidative addition of O–H of 3,5-difluorophenol to nickel was explored. Again, in the process of TS search and the optimization of a potential Ni–H species, it was shown that such Ni–H species could not be formed and that the H atom on Ni-center will add to olefin C=C bond upon geometry optimization, even if we started with a guess Ni–H structure.

8.5.4 Reductive elimination step

TS2B'	
$\Delta G^{\ddagger}$ = 5.9 [7.4]	

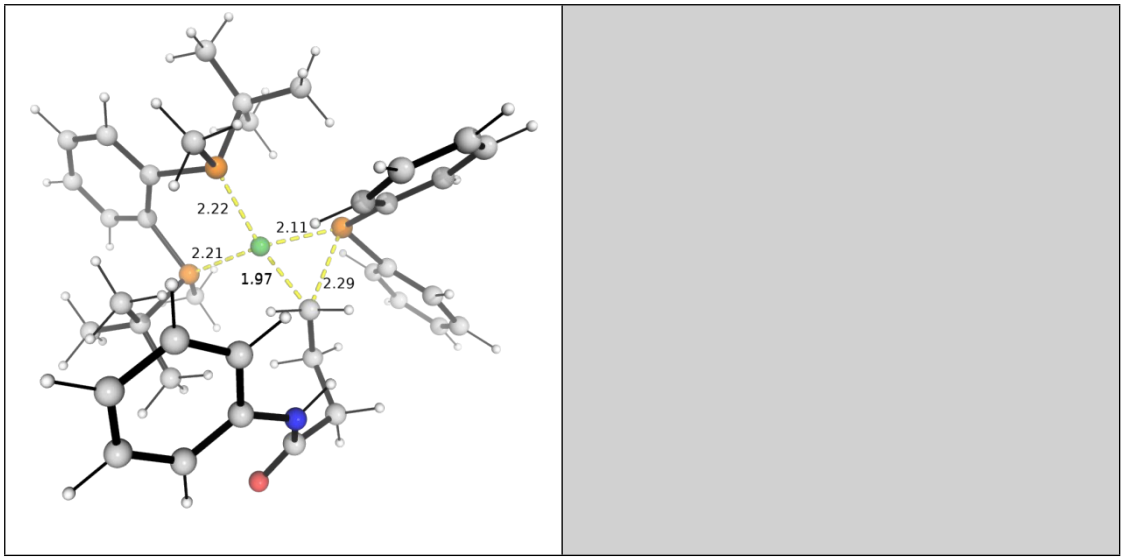

Figure S7. DFT-optimized structures of the reductive elimination step, **TS2B'**.

8.6 Estimation of product ratio under kinetic control

Under kinetic control, the product ratio of two pathways can be estimated using the ratio between the reaction rates of each pathway. The barrier difference ΔΔG‡ between two transition states gives a kinetic preference for the major product over the minor product. This can be estimated using simple transition state theory, without Boltzmann weighting of all the conformers via the following:

The Eyring equation

$$k = \frac{k_{\mathrm{B}}T}{h}\mathrm{e}^{-\Delta G^{\ddagger}/RT}$$

gives the rate constant under simple transition state theory (TST) assumptions.

Under kinetic control, as we compare the barrier heights difference between competing transition states, the ratio of the rates between two pathways is given by:

$$\frac{k_A}{k_B} = \frac{e^{-\Delta G_A^{\ddagger}/RT}}{e^{-\Delta G_B^{\ddagger}/RT}} = e^{-\Delta\Delta G^{\ddagger}/RT}$$

where k_X is the rate constant of pathway X (X=A or B); $\Delta G_X^{\ddagger}$ is the activation barrier for pathway X; and $\Delta\Delta G_X^{\ddagger}$ is the difference in the barrier heights; and R is the gas constant, T the temperature. Note that the Eyring Equation pre-exponential factor

cancels when comparing the ratio of the rate constants. Thus, using the calculated $\Delta\Delta G_X^{\ddagger}$ value (difference of barrier heights between competing TSs) at the reaction temperature (e.g., 80ºC = 353.15K), we are able to obtain the ratio of competing rates.

8.7 Optimized structures and absolute energies

Geometries of all optimized structures (in *.xyz* format with their associated gas-phase energy in Hartrees) are included in a separate folder named *DFT_optimized_structures*. All these data have been uploaded to https://zenodo.org/records/15683959 (DOI: 10.5281/zenodo.15683959).

Absolute values (in Hartrees) for SCF energy, zero-point vibrational energy (ZPE), enthalpy and quasi-harmonic Gibbs free energy (at 60ºC/333.15 K) for optimized structures are given below. Single point corrections in SMD THF using B3LYP-D3BJ/def2-TZVP level of theory are also included.

Structure	E/au	ZPE /au	H/au	T.S/ au	qh-G/au	SP CPCM(toluene-DMF)	SP SMD(toluene)
substrate1	-516.592634	0.189856	-516.38655	0.060904	-516.44473	-517.2216598	-517.2319173
HPPh2	-804.018129	0.19271	-803.80916	0.062175	-803.867969	-804.7180776	-804.7287202
NiCOD2	-2131.111086	0.364727	-2130.7223	0.072916	-2130.79436	-2132.101668	-2132.114489
difluorophenol	-505.014972	0.089438	-504.91475	0.046048	-504.960808	-505.6431965	-505.6481572
sulfonic_acid	-870.896284	0.104466	-870.77902	0.051952	-870.829978	-871.7189721	-871.7256604
PPh2_anion_opt	-803.445716	0.181289	-803.24856	0.059 17	-803.305954	-804.182809	-804.1999164

difluorophenol_anion_opt	-504.453006	0.075622	-504.36069	0.045653	-504.412552	-505.12693	-505.1378214
sulfonate_opt	-870.373325	0.0927	-870.26865	0.051076	-870.318368	-871.248698	-871.2592342
INT1	-3332.448935	0.59562	-3331.8039	0.129325	-3331.925897	-3334.386218	-3334.403416
INT1'	-3332.43917	0.595187	-3331.7941	0.132624	-3331.918195	-3334.377001	-3334.394991
INT1o	-3332.401125	0.593297	-3331.7577	0.134029	-3331.882434	-3334.339269	-3334.357009
INT2A	-4203.375226	0.702856	-4202.6102	0.158396	-4202.757197	-4206.125307	-4206.147158
TS1A_Cterm	-4203.371447	0.698973	-4202.6112	0.155936	-4202.756166	-4206.115919	-4206.137342
TS1A_Cterm_c2	-4203.370986	0.698922	-4202.6108	0.156075	-4202.755809	-4206.115423	-4206.136908
TS1A_Cterm_c3	-4203.363995	0.698512	-4202.6041	0.155799	-4202.749153	-4206.114602	-4206.136972
TS1A_Cterm_c4	-4203.367748	0.698772	-4202.6076	0.157093	-4202.753252	-4206.113239	-4206.135016
TS1A_Cterm_c5	-4203.364468	0.698062	-4202.6046	0.158028	-4202.751255	-4206.109129	-4206.132025
INT3A	-4203.377621	0.703734	-4202.6121	0.157735	-4202.758436	-4206.137644	-4206.160905
TS1A_Cin	-4203.354998	0.698316	-4202.5949	0.156848	-4202.741207	-4206.102639	-4206.124812
TS1A'_Cterm	-4203.350197	0.698221	-4202.5903	0.157513	-4202.73687	-4206.098504	-4206.121023
TS1A'_Cin	-4203.367163	0.698385	-4202.6072	0.156694	-4202.752956	-4206.11161	-4206.133187

TS1A'_Cin_c2	-4203.365757	0.698431	-4202.6057	0.156484	-4202.751453	-4206.109454	-4206.132154
TS1A'_Cin_c3	-4203.362332	0.698082	-4202.6025	0.158433	-4202.749226	-4206.106621	-4206.128325
INT4A	-4203.39806	0.70375	-4202.6324	0.159134	-4202.779735	-4206.146428	-4206.168536
INT5A	-4136.489952	0.794025	-4135.6301	0.164318	-4135.783115	-4139.118573	-4139.14416
TS2A	-4136.459567	0.792445	-4135.6014	0.1658	-4135.755049	-4139.091769	-4139.117576
INT6A	-4136.497856	0.793291	-4135.6383	0.168104	-4135.793237	-4139.138406	-4139.163894
TS1B_Cin	-3837.442905	0.681554	-3836.7006	0.156631	-3836.84548	-3840.000637	-3840.022279
TS1B_Cin_c2	-3837.44235	0.681913	-3836.6999	0.15739	-3836.844993	-3839.999114	-3840.02094
TS1B_Cin_c3	-3837.446679	0.682033	-3836.7044	0.152954	-3836.847112	-3840.001244	-3840.02122
TS1B_Cin_c4	-3837.441423	0.681571	-3836.6996	0.152833	-3836.842398	-3839.996732	-3840.016707
TS1B_Cterm	-3837.448687	0.683028	-3836.7057	0.151342	-3836.84772	-3840.005238	-3840.026502
TS1B'_Cterm	-3837.443629	0.681223	-3836.702	0.155481	-3836.846011	-3839.998488	-3840.019344
TS1B'_Cterm_c2	-3837.444553	0.6822	-3836.7021	0.152253	-3836.84458	-3839.998042	-3840.017653
TS1B'_Cterm_c3	-3837.443629	0.681224	-3836.702	0.155481	-3836.84601	-3839.998488	-3840.019345
INT2B'	-3837.484887	0.687263	-3836.7368	0.155675	-3836.881432	-3840.041245	-3840.061804

TS1B'_Cin	-3837.457574	0.68236	-3836.7152	0.152167	-3836.857526	-3840.013494	-3840.034225
TS1B'_Cin_c2	-3837.455155	0.681874	-3836.7131	0.152971	-3836.856155	-3840.00917	-3840.029164
TS1B'_Cin_c3	-3837.441656	0.681612	-3836.6993	0.157921	-3836.844441	-3839.998821	-3840.02013
INT3B'	-3837.462239	0.686306	-3836.7154	0.154204	-3836.858999	-3840.021633	-3840.043201
INT4B'	-3837.482346	0.688084	-3836.734	0.153141	-3836.876798	-3840.039563	-3840.06012
INT5B'	-4136.490165	0.795508	-4135.6295	0.164509	-4135.781562	-4139.122521	-4139.147995
TS2B'	-4136.46651	0.79201	-4135.6089	0.16606	-4135.76258	-4139.103329	-4139.129338
INT6B'	-4136.48813	0.793364	-4135.6284	0.168984	-4135.783697	-4139.130793	-4139.15707

9. Analytic data for the products

(*R*)-3-(diphenylphosphorothioyl)-N-phenylbutanamide (3a)

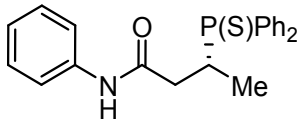

General procedure A was used with N-phenylbut-3-enamide **1a** (35.4 mg, 0.22 mmol, 2.2 equiv.) and diphenylphosphane **2a** (18.6 mg, 0.1 mmol, 1.0 equiv.) at 80 ℃ for 12 h to afford **3a** as foam (29.0 mg, 74% yield, 99% ee). ^{1}H NMR (400 MHz, Chloroform-*d*) δ 8.08-7.87 (m, 4H), 7.65 (s, 1H), 7.54-7.37 (m, 8H), 7.28-7.24 (m, 2H), 7.08 (t, *J* = 7.4 Hz, 1H), 3.62-3.49 (m, 1H), 2.70-2.44 (m, 2H), 1.17 (dd, *J* = 18.5, 6.8 Hz, 3H). ^{31}P NMR (162 MHz, Chloroform-*d*) δ 52.48. ^{13}C NMR (101 MHz, Chloroform-*d*) δ 168.95 (d, *J* = 16.0 Hz), 137.66, 131.74 (dd, *J* = 4.7, 2.9 Hz), 131.43 (dd, *J* = 9.6, 6.0 Hz), 130.65, 128.92 (d, *J* = 17.4 Hz), 128.84 (d, *J* = 23.1 Hz), 124.54, 119.85, 38.58 (d, *J* =

13. Rerference

1. Airiau, E.; Spangenberg, T.; Girard, N.; Schoenfelder, A.; Salvadori, J.; Taddei, M.; Mann, A., A general approach to aza-heterocycles by means of domino sequences driven by hydroformylation. *Chem. Eur. J.* **2008,** *14*, 10938-10948.
2. Derosa, J.; Kleinmans, R.; Tran, V. T.; Karunananda, M. K.; Wisniewski, S. R.; Eastgate, M. D.; Engle, K. M., Nickel-Catalyzed 1,2-Diarylation of Simple Alkenyl Amides. *J Am Chem Soc* **2018,** *140*, 17878-17883.
3. Nie, S. Z.; Davison, R. T.; Dong, V. M., Enantioselective Coupling of Dienes and Phosphine Oxides. *J. Am. Chem. Soc.* **2018,** *140*, 16450-16454.
4. Lee, C.; Kang, H. J.; Seo, H.; Hong, S., Nickel-Catalyzed Regio- and Enantioselective Hydroamination of Unactivated Alkenes Using Carbonyl Directing Groups. *J. Am. Chem. Soc.* **2022,** *144*, 9091-9100.
5. Yang, P.-F.; Liang, J.-X.; Zhao, H.-T.; Shu, W., Access to Enantioenriched 1,n-Diamines via Ni-Catalyzed Hydroamination of Unactivated Alkenes with Weakly Coordinating Groups. *ACS Catal.* **2022,** *12*, 9638-9645.
6. Yang, P.-F.; Zhu, L.; Liang, J.-X.; Zhao, H.-T.; Zhang, J.-X.; Zeng, X.-W.; Ouyang, Q.; Shu, W., Regio- and Enantioselective Hydroalkylations of Unactivated Olefins Enabled by Nickel Catalysis: Reaction Development and Mechanistic Insights. *ACS Catal.* **2022,** *12*, 5795-5805.
7. Wang, D. M.; She, L. Q.; Yuan, H.; Wu, Y.; Tang, Y.; Wang, P., Ligand-Enabled Ni(II) -Catalyzed Hydroxylarylation of Alkenes with Molecular Oxygen. *Angew. Chem. Int. Ed.* **2023,** *62*, e202304573.
8. Jankins, T. C.; Rubel, C. Z.; Ho, H. C.; Martin-Montero, R.; Engle, K. M., Tungsten-catalyzed stereodivergent isomerization of terminal olefins. *Chem. Sci.* **2025,** *16*, 2307-2315.
9. Nurseiit, A.; Janabel, J.; Gudun, K. A.; Kassymbek, A.; Segizbayev, M.; Seilkhanov, T. M.; Khalimon, A. Y., Bench-Stable Cobalt Pre-Catalysts for Mild Hydrosilative Reduction of Tertiary Amides to Amines and Beyond. *ChemCatChem* **2019,** *11*, 790-798.
10. Zhou, C.; Lei, T.; Wei, X.-Z.; Ye, C.; Liu, Z.; Chen, B.; Tung, C.-H.; Wu, L.-Z., Metal-Free, Redox-Neutral, Site-Selective Access to Heteroarylamine via Direct Radical–Radical Cross-Coupling Powered by Visible Light Photocatalysis. *J. Am. Chem. Soc.* **2020,** *142*, 16805-16813.
11. Grimme, S., Exploration of Chemical Compound, Conformer, and Reaction Space with Meta-Dynamics Simulations Based on Tight-Binding Quantum Chemical Calculations. *J. Chem. Theory Comput.* **2019,** *15*, 2847-2862.
12. Pracht, P.; Bohle, F.; Grimme, S., Automated exploration of the low-energy chemical space with fast quantum chemical methods. *Phys. Chem. Chem. Phys.* **2020,** *22*, 7169-7192.
13. Grimme, S.; Bannwarth, C.; Shushkov, P., A Robust and Accurate Tight-Binding Quantum Chemical Method for Structures, Vibrational Frequencies, and Noncovalent Interactions of Large Molecular Systems Parametrized for All spd-Block Elements (Z = 1-86). *J. Chem. Theory Comput.* **2017,** *13*, 1989-2009.

14. Bannwarth, C.; Ehlert, S.; Grimme, S., GFN2-xTB-An Accurate and Broadly Parametrized Self-Consistent Tight-Binding Quantum Chemical Method with Multipole Electrostatics and Density-Dependent Dispersion Contributions. *J. Chem. Theory Comput.* **2019,** *15*, 1652-1671.
15. Bannwarth, C.; Caldeweyher, E.; Ehlert, S.; Hansen, A.; Pracht, P.; Seibert, J.; Spicher, S.; Grimme, S., Extended tight-binding quantum chemistry methods. *Wiley Interdiscip. Rev. Comput. Mol. Sci.* **2021**, *11*, E1493.
16. Frisch, M. J et al., Gaussian 16, Revision B.01. 2016.
17. Yu, H. S.; He, X.; Li, S. L.; Truhlar, D. G., MN15: A Kohn–Sham global-hybrid exchange–correlation density functional with broad accuracy for multi-reference and single-reference systems and noncovalent interactions. *Chem. Sci.* **2016,** *7*, 5032-5051.
18. Weigend, F.; Ahlrichs, R., Balanced basis sets of split valence, triple zeta valence and quadruple zeta valence quality for H to Rn: Design and assessment of accuracy. *Phys. Chem. Chem. Phys.* **2005,** *7*, 3297-305.
19. Weigend, F., Accurate Coulomb-fitting basis sets for H to Rn. *Phys. Chem. Chem. Phys.* **2006,** *8*, 1057-65.
20. Achar, T. K.; Zhang, X.; Mondal, R.; Shanavas, M. S.; Maiti, S.; Maity, S.; Pal, N.; Paton, R. S.; Maiti, D., Palladium-Catalyzed Directed meta-Selective C-H Allylation of Arenes: Unactivated Internal Olefins as Allyl Surrogates. *Angew. Chem. Int. Ed.* **2019,** *58*, 10353-10360.
21. Guin, S.; Dolui, P.; Zhang, X.; Paul, S.; Singh, V. K.; Pradhan, S.; Chandrashekar, H. B.; Anjana, S. S.; Paton, R. S.; Maiti, D., Iterative Arylation of Amino Acids and Aliphatic Amines via delta-C(sp(3))-H Activation: Experimental and Computational Exploration. *Angew. Chem. Int. Ed.* **2019,** *58*, 5633-5638.
22. Porey, S.; Zhang, X.; Bhowmick, S.; Kumar Singh, V.; Guin, S.; Paton, R. S.; Maiti, D., Alkyne Linchpin Strategy for Drug:Pharmacophore Conjugation: Experimental and Computational Realization of a Meta-Selective Inverse Sonogashira Coupling. *J. Am. Chem. Soc.* **2020,** *142*, 3762-3774.
23. Sinha, S. K.; Panja, S.; Grover, J.; Hazra, P. S.; Pandit, S.; Bairagi, Y.; Zhang, X.; Maiti, D., Dual Ligand Enabled Nondirected C-H Chalcogenation of Arenes and Heteroarenes. *J. Am. Chem. Soc.* **2022,** *144*, 12032-12042.
24. Das, J.; Ali, W.; Ghosh, A.; Pal, T.; Mandal, A.; Teja, C.; Dutta, S.; Pothikumar, R.; Ge, H.; Zhang, X.; Maiti, D., Access to unsaturated bicyclic lactones by overriding conventional C(sp(3))-H site selectivity. *Nat. Chem.* **2023,** *15*, 1626-1635.
25. Dutta, U.; Prakash, G.; Devi, K.; Borah, K.; Zhang, X.; Maiti, D., Directing group assisted para-selective C-H alkynylation of unbiased arenes enabled by rhodium catalysis. *Chem. Sci.* **2023,** *14*, 11381-11388.
26. Porey, S.; Bairagi, Y.; Guin, S.; Zhang, X.; Maiti, D., Nondirected C–H/C–F Coupling for the Synthesis of α-Fluoro Olefinated Arenes. *ACS Catal.* **2023,** *13*, 14000-14011.
27. Bairagi, Y.; Porey, S.; Vummaleti, S. V. C.; Zhang, X.; Lahiri, G. K.; Maiti, D., Synthesis of β-(Hetero)aryl Ketones via Ligand-Enabled Nondirected C–H Alkylation. *ACS Catal.* **2024,** *14*, 15654-15664.

28. Barone, V.; Cossi, M., cossi-barone-1998-quantum-calculation-of-molecular-energies-and-energy-gradients-in-solution-by-a-conductor-solvent. *J. Phys. Chem. A* **1998,** *102*, 1995-2001.
29. Cossi, M.; Rega, N.; Scalmani, G.; Barone, V., Energies, structures, and electronic properties of molecules in solution with the C-PCM solvation model. *J. Comput. Chem.* **2003,** *24*, 669-681.
30. Boruah, A.; Boro, B.; Wang, J.; Paul, R.; Ghosh, R.; Mohapatra, D.; Li, P. Z.; Zhang, X.; Mondal, J., Influence of Keto-Enol Tautomerism in Regulating CO(2) Photoreduction Activity in Porous Organic Porphyrinic Photopolymers. *ACS Appl. Mater. Interfaces* **2025,** *17*, 1259-1272.
31. Grimme, S., Supramolecular binding thermodynamics by dispersion-corrected density functional theory. *Chem. Eur. J.* **2012,** *18*, 9955-9964.
32. Luchini, G.; Alegre-Requena, J. V.; Funes-Ardoiz, I.; Paton, R. S., GoodVibes: automated thermochemistry for heterogeneous computational chemistry data. *F1000Research* **2020,** *9*.
33. Bryantsev, V. S.; Diallo, M. S.; Goddard III, W. A., Calculation of Solvation Free Energies of Charged Solutes Using Mixed Cluster/Continuum Models. *J. Phys. Chem. B* **2008,** *112*, 9709-9719.
34. Schrödinger, L. The PyMOL Molecular Graphics Development Component, Version 1.8; 2015.
35. Ess, D. H.; Houk, K. N., Distortion-interaction-energy-control-of-1-3-dipolar-cycloaddition-reactivity. *J. Am. Chem. Soc.* **2007**, 10646-10647.
36. Bickelhaupt, F. M.; Houk, K. N., Analyzing Reaction Rates with the Distortion/Interaction-Activation Strain Model. *Angew. Chem. Int. Ed.* **2017,** *56*, 10070-10086.

Full reference Gaussian 16:

Gaussian 16, Revision B.01, Frisch, M. J.; Trucks, G. W.; Schlegel, H. B.; Scuseria, G. E.; Robb, M. A.; Cheeseman, J. R.; Scalmani, G.; Barone, V.; Mennucci, B.; Petersson, G. A.; Nakatsuji, H.; Caricato, M.; Li, X.; Hratchian, H. P.; Izmaylov, A. F.; Bloino, J.; Zheng, G.; Sonnenberg, J. L.; Hada, M.; Ehara, M.; Toyota, K.; Fukuda, R.; Hasegawa, J.; Ishida, M.; Nakajima, T.; Honda, Y.; Kitao, O.; Nakai, H.; Vreven, T.; Montgomery Jr., J. A.; Peralta, J. E.; Ogliaro, F.; Bearpark, M.; Heyd, J. J.; Brothers, E.; Kudin, K. N.; Staroverov, V. N.; Kobayashi, R.; Normand, J.; Raghavachari, K.; Rendell, A.; Burant, J. C.; Iyengar, S. S.; Tomasi, J.; Cossi, M.; Rega, N.; Millam, J. M.; Klene, M.; Knox, J. E.; Cross, J. B.; Bakken, V.; Adamo, C.; Jaramillo, J.; Gomperts, R.; Stratmann, R. E.; Yazyev, O.; Austin, A. J.; Cammi, R.; Pomelli, C.; Ochterski, J. W.; Martin, R. L.; Morokuma, K.; Zakrzewski, V. G.; Voth, G. A.; Salvador, P.; Dannenberg, J. J.; Dapprich, S.; Daniels, A. D.; Farkas, Ö.; Foresman, J.

B.; Ortiz, J. V; Cioslowski, J.; Fox, D. J. Gaussian, Inc., Wallingford CT, 2016.